Electronic structure of C_{84} film studied by photoemission measurement and first-principles calculation

2009 J. Phys.: Condens. Matter 21 265502

(http://iopscience.iop.org/0953-8984/21/26/265502)

J. Phys.: Condens. Matter **21** (2009) 265502 (6pp) doi:10.1088/0953-8984/21/26/265502

Electronic structure of C_{84} film studied by photoemission measurement and first-principles calculation

Hong-Nian Li[1,5], Hua Yang[2], Xiao-Xiong Wang[3], Jing-Fu Ni[1], Peng Wang[1], Liang Meng[1], Xiao-Bo Wang[1], Ibrahim Kurash[4], Hai-Jie Qian[4], Jia-Ou Wang[4] and Zi-Yang Liu[2]

[1] Department of Physics, Zhejiang University, Hangzhou 310027, People's Republic of China
[2] Department of Chemistry, Zhejiang University, Hangzhou 310027, People's Republic of China
[3] College of Science, Nanjing University of Science and Technology, Nanjing 210094, People's Republic of China
[4] Laboratory of Synchrotron Radiation, Institute of High Energy Physics, Chinese Academy of Sciences, Beijing 100039, People's Republic of China

E-mail: Phylihn@public.zju.edu.cn

Received 18 January 2009, in final form 29 March 2009
Published 5 June 2009
Online at stacks.iop.org/JPhysCM/21/265502

Abstract

We have measured the photoemission spectra of a C_{84} film (isomer mixture) with synchrotron radiation. The valence band exhibits abundant spectral features from the Fermi level to ~18 eV binding energy. The relative intensity between the lowest binding energy feature (labeled as A) and the next lowest binding energy feature (labeled as B) oscillates distinctly within the experimental photon energy region from 21.0 to 63.0 eV. The energy levels and density of states (DOS) are calculated for the $D_{2d}(23)$-C_{84} and four D_2 symmetric ($D_2(1)$, $D_2(5)$, $D_2(21)$ and $D_2(22)$) C_{84} isomers to help us to understand the electronic structure. The experimental features and the theoretical DOS peaks have one-to-one correspondence. The number of electrons occupying the states of feature A is 12 or 13.3, depending on the different kinds of isomer mixtures. The electron occupation of feature B is 18.67 e. With the spherical symmetric approximation, features A and B can be characterized with angular momenta of 6 and 5, respectively. The angular momentum difference is the reason for the photoelectron intensity oscillations.

1. Introduction

Although C_{84} is the third most abundant fullerene, its yield in the arc-processed soot [1] was not yet high enough to make possible extensive studies in past years. This situation may be altered in the near future, as commercial C_{84} has become available. The C_{84} sample available for most researchers consists of two isomers of D_2 and D_{2d} symmetries with a 2:1 abundance ratio, as was rather reliably determined by the comparison between the nuclear magnetic resonance (NMR) data [2] and the theoretical numbers and intensities of the NMR lines [3]. The D_{2d} symmetric isomer was identified experimentally [4] to be the $D_{2d}(23)$-C_{84} (the notation of '23' is after [3]), but the D_2 symmetric isomer has not been unambiguously assigned to one of the four possible candidates ($D_2(1)$-C_{84}, $D_2(5)$-C_{84}, $D_2(21)$-C_{84} and $D_2(22)$-C_{84}), although the $D_2(22)$-C_{84} was recommended by some theoretical calculations [5–7] and a scanning tunneling microscopy (STM) study [8]. Probably owing to the very similar structural and chemical properties of the isomers, C_{84} can be crystallized with sharp x-ray diffraction peaks [9]. We can thus expect some novel properties of solid C_{84} and its compounds. Indeed, the metallic phase of metal-intercalated C_{84} ($Rb_{8.8}C_{84}$) has been found [10]. For the purpose of predicting and understanding the properties of C_{84} and its

[5] Author to whom any correspondence should be addressed.

compounds, the knowledge about the electronic structure of C_{84} is needed.

There have been some works [11–13] that reported the photoemission (PES) data for part of the region, 0–12 eV binding energy (BE), of the valence band of C_{84}. The calculated energy level diagrams and density of states (DOSs) for $D_2(1)$-C_{84}, $D_2(22)$-C_{84} [7] and $D_{2d}(23)$-C_{84} [7, 10, 14] have also been reported. Saito *et al* [15] compared the DOSs with the PES data [11] for the three lowest binding energy features. However, the assignments of the photoemission features to particular molecular orbital-derived bands have not been achieved up to now due to the sophisticated energy level structures [7, 10, 14] and the scarcity of the comparison between calculated levels and PES data in the large binding energy region (e.g. the entire valence band). Sufficiently detailed energy level diagrams for the unoccupied electronic states of the D_2 symmetric isomers, which are indispensable for analyses of the experimental data (PES, x-ray absorption spectrum, transport property, etc) of C_{84} compounds, have not been reported.

The aim of the present work is to afford sufficient and self-contained knowledge of the valence band of C_{84} for future work. We carried out PES measurements of a C_{84} film and performed first-principles calculations of C_{84} molecules. In the PES measurements, we measured a spectrum of the entire occupied valence band (from the Fermi level to ∼27.5 eV BE) and the detailed evolution of the spectrum with photon energies from 21.0 to 63.0 eV with increments of 2.0 eV. In the first-principles calculations, we calculated the energy levels and the DOSs for the $D_{2d}(23)$-C_{84} and all four D_2 symmetric isomers. The comparison between the experimental data and the theoretical results are made to give a deep understanding of the electronic structure of C_{84}.

2. Experimental and calculation details

C_{84} was synthesized by the conventional arc discharge of a graphite stick in an He atmosphere of 15 kPa. The as-produced raw soot was dissolved in dichlorobenzene, ultrasonicated for 8 h and filtered with the aid of minus atmosphere (low vacuum). The extractant was then removed into toluene from dichlorobenzene using the vaporization distilling method, for isolation using high performance liquid chromatograph (HPLC). The HPLC profile of our sample exhibits the signal of C_{84} only, in comparison with the commercial C_{84} (99%, BuckyUSA, Houston, TX, USA) which exhibits a noticeable signal of C_{78}. The solid C_{84} obtained from the eluent was further purified by degassing at 300 °C in a high vacuum system (10^{-6} mbar) for 24 h to evaporate the residual solvent.

Synchrotron radiation photoemission measurements were carried out in the Photoelectron Spectroscopy Station of the Beijing Synchrotron Facility (BSRF). The low energy branch of the beamline produces light with photon energies from 15 to 65 eV for angle-resolved photoemission (ARPES) measurements, and three high energy branches afford photons with energies from 60 to 1000 eV for angle integrated photoemission (AIPES) measurements. Thoroughly degassed

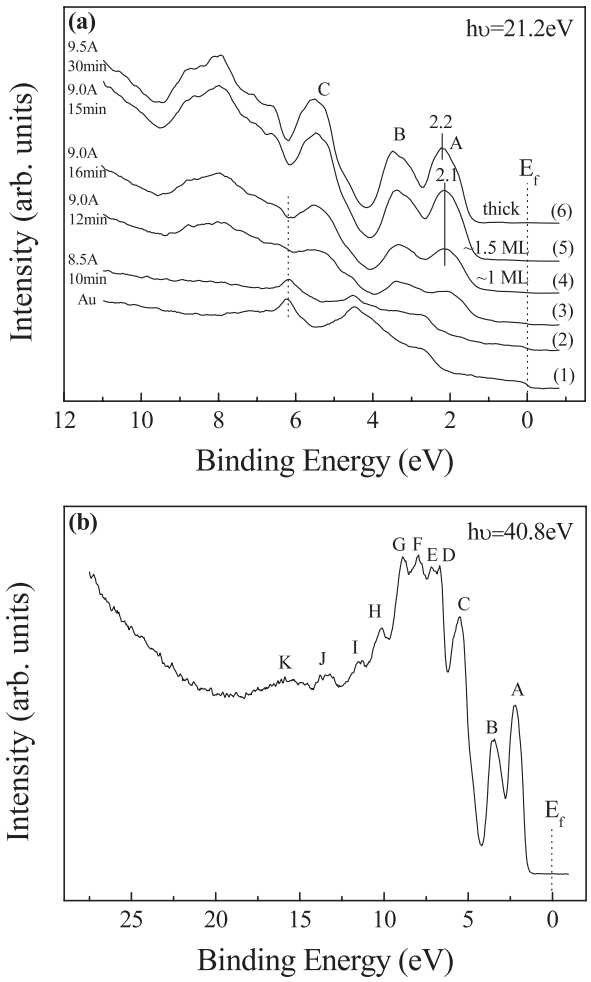

Figure 1. (a) Photoemission spectra of C_{84} overlayers on Au film measured with the photon energy of 21.2 eV. The deposition time and the currents through the Ta boat for each deposition round are indicated next to the lines. The spectra are normalized to the incident photon flux. (b) The spectrum of thick C_{84} film measured with the photon energy of 40.8 eV.

C_{84} was sublimed from a Ta boat located at about 11 cm from an Au film substrate. The substrate was cleaned by cycles of Ar ion bombarding and annealing at ∼550 °C until C 1s and O 1s signals could not be observed by AIPES ($h\upsilon = 650$ eV) measurements. The amount of C_{84} deposited onto the substrate was controlled by the electric current through the Ta boat and deposition time. We measured the ARPES of the sample with relatively high resolution (∼0.1 eV) for two typical photon energies, 21.2 and 40.8 eV, by adjusting the pass energy of the energy analyzer and the width of the slit of the beamline. In the measurements of the photon-energy-dependent spectra ($h\upsilon = 21.0$–63.0 eV), we moderately decreased the resolution to reduce the experimental time. All the spectra were measured at normal emission.

The first-principles calculations were performed with the DMol^3 package [16, 17] based on density functional theory (DFT). The functional adopted in this work is the BLYP [18, 19] generalized gradient approximation (GGA) functional. All electron calculations were performed with the double numerical basis sets plus polarization functional (DNP),

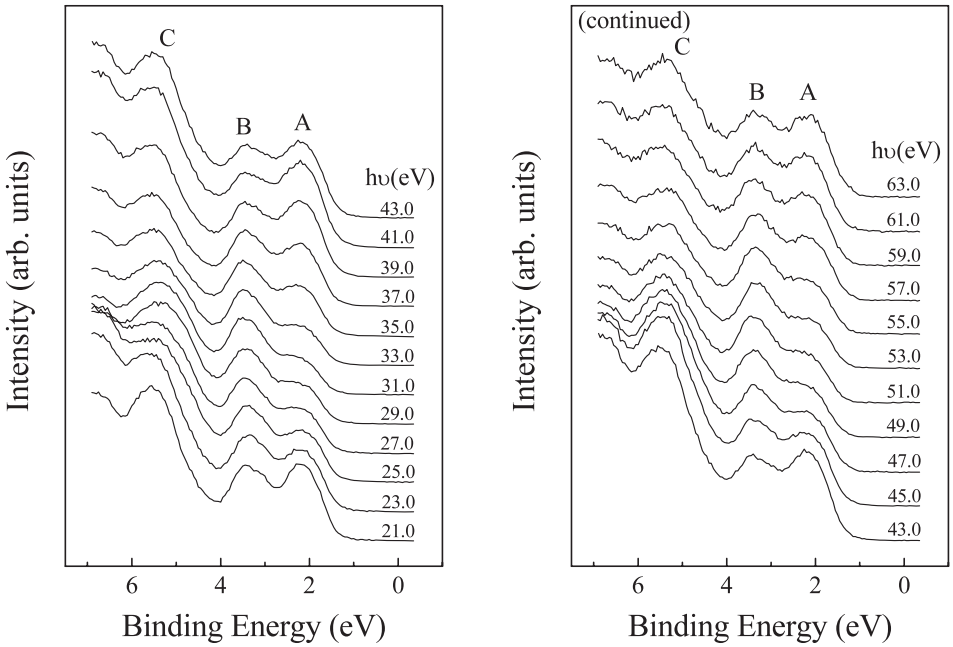

Figure 2. Photoemission spectra of C_{84} film measured with different photon energies from 21.0 eV to 63.0 eV. The spectral lines are normalized to the height of feature B.

i.e. functions with angular momentum one higher than that of the highest occupied orbital in the free atom. The orbital cutoff was 3.7 Å. Self-consistent field procedures were carried out with a convergence criterion of 10^{-6} au on the energy and electron density. Geometry optimizations were performed with a convergence criterion of 10^{-5} on the energy, 10^{-4} on the gradient and 10^{-3} on the displacement.

3. Results and discussion

Figure 1(a) determines the binding energy of the spectrum with reference to the Au Fermi edge. The bottom line is the spectrum of a clean Au film. The signal intensity of C_{84} increases monotonically with more molecules deposited onto the substrate from line (2) to line (5), and then kept nearly invariant. The signal of the substrate is still discernible in line (4). The dip at ∼6.2 eV in line (4) is rather shallow compared with that in line (5), which is the contribution of the Au 5d signal as indicated by the dotted vertical line in the figure. In analogy to the case of monolayer C_{60} on Ag(111) [20], where the substrate contributed about 1/5 of the signal to the total spectral intensity at the photon energy (21.0 eV) near that adopted in figure 1(a), we roughly estimate the coverage of C_{84} for line (4) as being near 1 ML. According to the deposition time, the coverage for line (5) is ∼1.5 ML. The coverage for line (6), which is denoted by 'thick', cannot be quantitatively estimated because we increased the electric current through the Ta boat from 9.0 to 9.5 A. It seems that the amount of charge transfer from Au to C_{84} is very small because the spectral weight between the Fermi level and ∼1.3 eV BE is very weak in the ∼1 ML spectrum. Lines (5) and (6) are nearly the same as the spectrum of C_{84} reported in [12]. The absence of photoemission between the Fermi level and ∼1.3 eV binding energy indicates the semiconducting property of the C_{84} film. Three features with the lowest binding energies are labeled by A, B and C in the figure. The binding energy of feature A is 2.1 eV for the coverages near 1 ML (the same as that of [12]), and changes to be 2.2 eV for line (6) due to the slight charging effect of the non-conducting C_{84} thick film.

The entire occupied valence band measured on the thick film sample with the photon energy of 40.8 eV is shown in figure 1(b). Compared to the spectra measured with the lower photon energy such as 21.2 eV (figure 1(a) and [11–13]), figure 1(b) exhibits more abundant and more distinct spectral features. The valence band shows eleven evident peaks up to 18 eV BE (labeled by A, B, . . ., K) and some shoulders. These spectral features reveal that the electronic structure of the C_{84} film retains much of the molecular character, i.e. the intra-molecular binding is distinctly stronger than the inter-molecular interaction. Therefore the spectrum can be understood, to a large extent, with the help of the molecular orbital calculations.

Figure 2 exhibits the photon-energy-dependent spectra, which affords more information about the electronic structure and will help in the comparison between the experimental data and the calculated results. The relative intensity between features A and B varies distinctly with photon energies, as was already observed by Hino *et al* [11]. Our data measured with smaller energy increments (2.0 eV) in a relatively larger photon energy region (21.0–63.0 eV) can find that the relative intensity oscillates regularly, as in the case of C_{60} [21, 22]. The intensity ratio between features A and B exhibits three maxima (at 21.0, 41.0 and 63.0 eV) and two minima (at 31.0 and 53.0 eV) within the photon energy region of the present work. The seeming shift of the peak position of feature C around $h\upsilon = 27.0$ eV is most possibly due to the photoelectron intensity variations of different molecular orbitals constituting this feature.

Figure 3 displays the calculated energy level diagrams and the theoretical DOSs for the five C_{84} isomers. The dotted lines in the figure separate the occupied and the unoccupied states. Considering the facts that larger fullerene molecules (C_{84} [10] or C_{70} [23]) can combine with up to nine metal ions in the fullerides, we show in figure 3(a) nine unoccupied levels (the twofold-degenerate level of $D_{2d}(23)$-C_{84} is taken as two levels) together with their symmetries for each isomer to help to study the divalent metal (alkaline-earth and rare-earth metals) intercalated C_{84} in the future. The energy gaps between the lowest unoccupied molecular orbital (LUMO) and the highest occupied molecular orbital (HOMO) are 1.351 eV, 0.985 eV, 0.530 eV, 1.032 eV and 1.094 eV for the $D_2(1)$-C_{84}, $D_2(5)$-C_{84}, $D_2(21)$-C_{84}, $D_2(22)$-C_{84} and $D_{2d}(23)$-C_{84}, respectively (the lengthy notations of the isomers will sometimes be abbreviated to (1), (5), etc, in the following). The arrows indicate the selection-rule-allowable transitions (between identical irreducible representations). For isomers (1), (21) and (22), the energy intervals indicated beside the arrows, rather than the LUMO–HOMO gaps, should be used to compare with the optical absorption spectra [10]. Considering the measured optical gap of ∼1.1 eV [10], isomers (5) and (21) seem not to be the candidate of the D_2 symmetric isomer in the sample. However, it is well known that the DFT calculation has some uncertainties in the energy intervals. The comparison between the calculated results and the PES data in the following will reveal that the energy intervals of the calculated results are underestimated. The actual optical gaps may be no less than ∼1.1 eV for all these isomers. Therefore we have to take into consideration all four D_2 symmetric isomers at present. The DOSs of these isomers shown in figure 3(b) are obtained by Gaussian convolution of the discrete energy levels and summation over them. For comparing with the experimental data, we adopt the full width at half-maximum (FWHM) of 0.3 eV for the Gaussian lines to simulate the energy resolution of the PES measurement and the solid broadening effect.

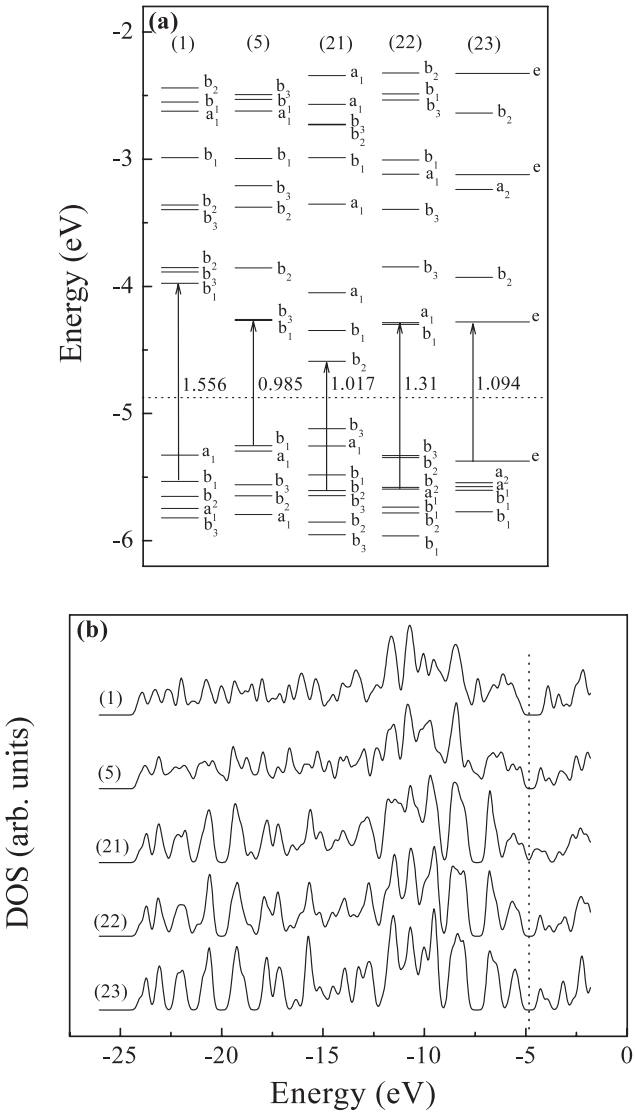

Figure 3. DFT calculation results of five C_{84} isomers (nos. (1), (5), (21), (22) and (23)). (a) Energy level diagrams. The symmetries (irreducible representations of the D_2 and D_{2d} point groups) for each level are shown. The horizontal dotted line separates the occupied and the unoccupied levels, and the vertical arrows indicate the smallest energy intervals of the symmetry allowable transitions. (b) Density of states of the C_{84} isomers. The DOSs are obtained by Gaussian convolution (FWHM = 0.3 eV) of the discrete energy levels and summation over them. The vertical dotted line separates the occupied and the unoccupied states.

The comparison between the experimental spectrum (figure 1(b)) and the theoretical DOSs is shown in figure 4. We constructed the DOSs by summing the DOSs of the D_2 symmetric C_{84} and the $D_{2d}(23)$-C_{84} in figure 3(b) with a component ratio of 2:1. The energy of the resulting DOSs was changed to be positive to match the habit of PES (giving the binding energy as a positive number), and then shifted (by −3.34 eV) to make the DOSs coincide with spectral feature A. All the experimental features can find their theoretical counterparts. The DOS peaks with binding energies larger than 18 eV cannot be observed experimentally, probably due to the matrix element effect. However, a DOS peak at low binding energy (∼4 eV, see the arrow in figure 4) of the (23) + 2 × (1) isomer mixture, has no counterpart in the experimental spectrum. The DOS peak cannot yet be observed in the photon-energy-dependent spectra in figure 2, indicating that the absence of this peak is not due to the matrix element effect. Therefore we preclude the $D_2(1)$-C_{84} as a component of the C_{84} sample. Despite the general coincidence, the energy intervals between the DOS peaks are shrunken as compared with the experimental data. This disagreement is due to the shortcoming of the DFT calculation. It is well known that the accuracy of the DFT calculation is limited (mainly) by the approximation of the exchange–correlation functionals. The BLYP functional used in this work, though superior to the local density approximation (LDA) by taking into account the gradient of the density at each point, does not adequately incorporate the long-range correlation. The calculated results need some remedy to compare with the experimental data in more detail.

We found that multiplying the energy scale by a coefficient of 1.117 can make the theoretical DOSs coincide with the experimental data much better, as shown in figure 5. The

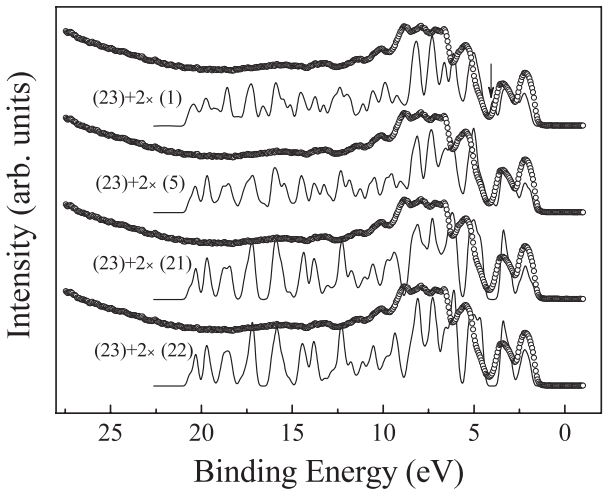

Figure 4. Comparison between the experimental data (open circles) and the theoretical DOSs. The theoretical DOS is the combination of the DOSs of the D_2 symmetric C_{84} and the $D_{2d}(23)$-C_{84} with a weight of 2:1.

coefficient of 1.117 may be a meaningful empirical correction to the DFT calculation compensating for the shortcoming of the BLYP functional. The DOS of the (23) + 2 × (1) isomer mixture has been excluded from the figure. The DOSs of all the remaining isomer mixtures seem to coincide with the experimental data fairly well. Closer inspection of the figure can find that the (23) + 2 × (22) mixture coincides with the spectrum best. Figure 5(b) enlarges the comparison for this mixture. Not only the PES peaks (vertical solid lines) but also the shoulders (vertical dotted line) have their theoretical counterparts with very good binding energy coincidence. We do not compare the intensities because of the matrix element effect. The experimental peak E is not reproduced in the calculated DOS of the (23) + 2 × (21) mixture and the position of peak H has some discrepancy from the calculated result of the (23) + 2 × (5) mixture. Taking into account the validity of the comparison affected by the multiplying coefficient (1.117) and the matrix element effect, we cannot yet readily draw the conclusion of the (23) + 2 × (22) mixture being the actual components of the C_{84} sample. Whatever the actual sample components are, figures 5(a) and (b) reveal that we can ascribe the PES features to bunches of molecular energy levels with satisfying accuracy, which will be further discussed for features A and B in the following.

Figure 5(c) compares the PES features A and B with the calculated energy levels of the $D_2(5)$, $D_2(21)$, $D_2(22)$ and $D_{2d}(23)$ isomers. The energy levels have also been multiplied by 1.117 in energy scale and displaced the same as in figure 5(a). We can draw information on electron occupation and angular momentum properties from this figure. By counting the number of energy levels corresponding to feature B, one immediately finds that the average electron occupation is 18.67 e (= (2 × 18 e + 1 × 20 e)/3), irrespective of which D_2 symmetric isomer is the actual component. The average electron occupation of feature A is 12 e for the (23) + 2 × (5) mixture or 13.3 e for the (23) + 2 × (21) and (23) + 2 × (22) mixtures. The angular momentum properties

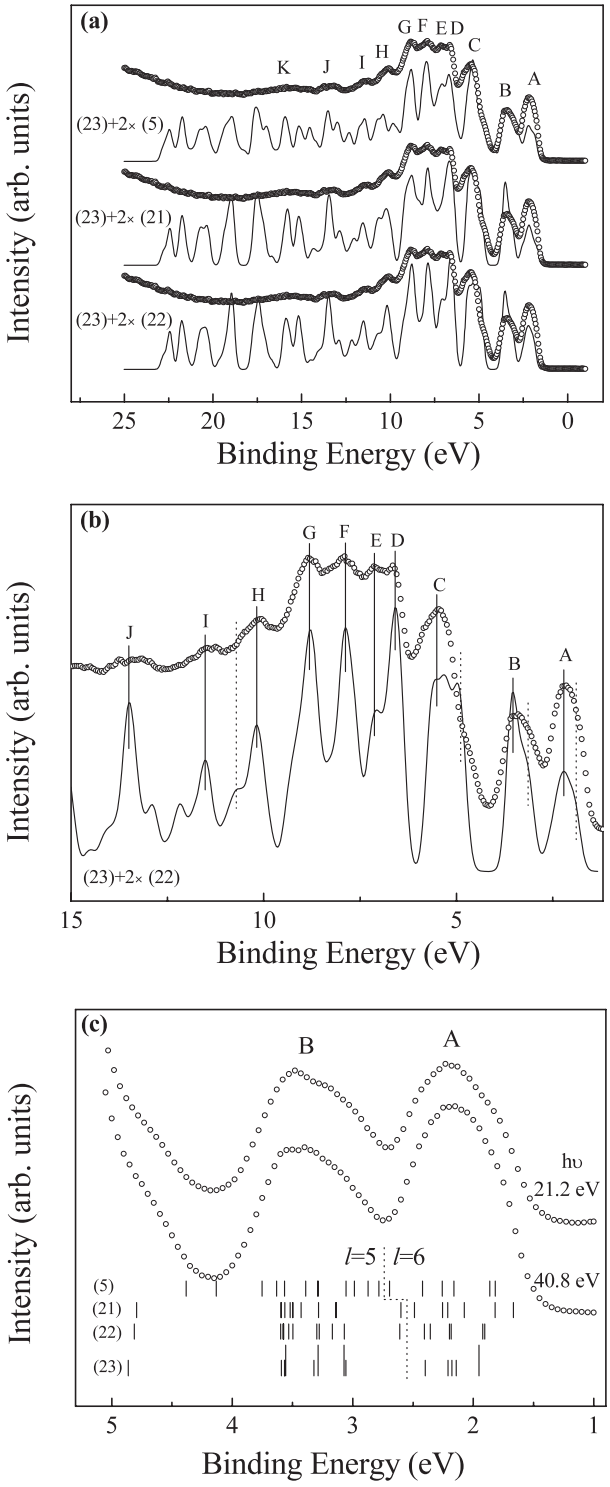

Figure 5. (a) Comparison between the experimental data and the calculated theoretical DOSs (multiplied by a coefficient of 1.117 in energy scale). (b) Enlarged view of the comparison for the (23) + 2 × (22) mixture. (c) Assignments of spectral features A and B to particular molecular orbitals. The energy levels have also been multiplied by the same coefficient of 1.117 in energy scale as in (a). The dotted lines separate the energy levels with different angular momenta.

of features A and B can be obtained by analogy with the case of C_{60} [24]. The detailed wavefunction analyses of C_{60} [24] revealed that the electronic structure can be described fairly

well with the spherical symmetric approximation, i.e. most of the energy levels correspond to one dominant (greater than 90% contribution) angular momentum. It was also revealed that the electronic states around the Fermi level (from ~4.5 eV BE to several electronvolts above the Fermi level in the PES and inverse photoemission spectra (IPES)) are of π character [24]. Since isomers (5), (21), (22) and (23) have near-spherical shapes (though slightly lower symmetric than C_{60}) [4], we can expect that the energy levels of C_{84} are also characterized with specific angular momenta and that the PES features A and B be of π character. Among the 84 π electrons, 50 electrons occupy the states with angular momenta $l = 0$–4, 22 electrons occupy the states with $l = 5$ and the remaining 12 electrons have an angular momentum of $l = 6$. In figure 5(c), the six highest occupied levels of each isomer should have an angular momentum of 6, and the next eleven occupied levels have an angular momentum of 5. Therefore feature B can be characterized with $l = 5$. For feature A, the angular momentum is 6 for the $23 + 2 \times (5)$ mixture or is dominated by $l = 6$ with a minor (10%) contribution of $l = 5$ for the $23 + 2 \times (22)$ and $23 + 2 \times (21)$ mixtures. Owing to the sophisticated energy level structures of features A and B (in comparison to the single-energy-level-derived HOMO band and the two-energy-level-derived HOMO-1 band of C_{60} [24]) and the relatively lower symmetric shapes of C_{84} molecules, the above discussions about the angular momentum properties need verification by further theoretical work. However, we believe the conclusions on the angular momenta of features A and B are basically correct since it is consistent with the observation of the photoelectron intensity oscillations. With the spherical symmetric approximation, the maxima of the photoelectron intensity of feature A should correspond to the minima of feature B (and vice versa) because the radial wavefunction (spherical Bessel function) giving rise to the oscillatory behavior in this model has a phase shift of π between odd and even angular momenta of the outgoing photoelectron wave [22, 25]. Therefore we can observe the obvious oscillations of the relative intensity in figure 2.

4. Conclusions

The valence band of C_{84} exhibits abundant photoemission features from the Fermi level to ~18 eV BE. The assignment of these features to particular bunches of energy levels is achieved by first-principles calculations. Detailed energy level diagrams for the unoccupied states are given, which are capable of helping the study of C_{84} compounds. The electron occupations and the angular momenta are determined for two lowest binding energy features (A and B). The relative photoelectron intensity of features A ($l = 6$) and B ($l = 5$) oscillates distinctly with photon energies because of the angular momentum difference.

Acknowledgments

This work is supported by the National Natural Science Foundation of China under no. 10674115 and the Beijing Synchrotron Radiation Facility.

References

[1] Diederich F *et al* 1991 *Science* **252** 548
[2] Kikuchi K, Nakahara N, Wakabayashi T, Suzuki S, Shiromaru H, Miyake Y, Saito K, Ikemoto I, Kainosho M and Achiba Y 1992 *Nature* **357** 142
[3] Manolopoulos D E and Fowler P W 1992 *J. Chem. Phys.* **96** 7603
[4] Dennis T J S, Kai T, Tomiyama T and Shinohara H 1998 *Chem. Commun.* 619
[5] Zhang B L, Wang C Z and Ho K M 1992 *J. Chem. Phys.* **96** 7183
[6] Bakowies D, Kolb M, Thiel W, Richard S, Ahlrichs R and Kappes M M 1992 *Chem. Phys. Lett.* **200** 411
[7] Wang X Q, Wang C Z, Zhang B L and Ho K M 1992 *Phys. Rev. Lett.* **69** 69
[8] Wang X D, Hashizume T, Shinohara H, Saito Y, Nishina Y and Sakurai T 1993 *Phys. Rev.* B **47** 15923
[9] Margadonna S, Brown C M, Dennis T J S, Lappas A, Pattison P, Prassides K and Shinohara H 1998 *Chem. Mater.* **10** 1742
[10] Rikiishi Y *et al* 2005 *Phys. Rev.* B **71** 224118
[11] Hino S *et al* 1992 *Chem. Phys. Lett.* **190** 169
[12] Armbruster J F *et al* 1994 *Phys. Rev.* B **50** 4933
[13] Ito A, Akaki O and Takahashi T 1996 *J. Electron Spectrosc. Relat. Phenom.* **78** 457
[14] Wu H, Deng K, Lu G, Yuan Y, Yang J and Wang X 2006 *J. Phys.: Condens. Matter* **18** 7115
[15] Saito S, Sawada S, Hamada N and Oshiyama A 1993 *Mater. Sci. Eng.* B **19** 105
[16] Delley B 1990 *J. Chem. Phys.* **92** 508
[17] Delley B 2000 *J. Chem. Phys.* **113** 7756
[18] Becke A D 1988 *J. Chem. Phys.* **88** 1053
[19] Lee C, Yang W and Parr R G 1988 *Phys. Rev.* B **37** 785
[20] Li H N, Wang X X, He S L, Kurash I, Qian H J, Su R, Zhong J, Abbas M I and Hong C H 2005 *Surf. Sci.* **586** 65
[21] Benning P J, Poirier D M, Troullier N, Martins J L, Weaver J H, Haufler R E, Chibante L P F and Smalley R E 1991 *Phys. Rev.* B **44** 1962
[22] Wang X X, Xu Y B, Li H N, Zhang W H and Xu F Q 2008 *J. Electron Spectrosc. Relat. Phenom.* **165** 20
[23] Takenobu T, Chi D H, Margadonna S, Prassides K, Kubozono Y, Fitch A N, Kato K and Iwasa Y 2003 *J. Am. Chem. Soc.* **125** 1897
[24] Troullier N and Martins J L 1992 *Phys. Rev.* B **46** 1754
[25] Xu Y B, Tan M Q and Becker U 1996 *Phys. Rev. Lett.* **76** 3538